Geomorphology 306 (2018) 90–101

Contents lists available at ScienceDirect

Geomorphology

journal homepage: www.elsevier.com/locate/geomorph

Can glacial shearing of sediment reset the signal used for luminescence dating?

Mark D. Bateman [a,*], Darrel A. Swift [a], Jan A. Piotrowski [b], Edward J. Rhodes [a], Anders Damsgaard [b,1]

[a] Department of Geography, University of Sheffield, UK
[b] Department of Geoscience, Aarhus University, Denmark

ARTICLE INFO

Article history:
Received 2 August 2017
Received in revised form 19 January 2018
Accepted 19 January 2018
Available online 4 February 2018

Keywords:
Glacial grinding
Shear stress
Luminescence

ABSTRACT

Understanding the geomorphology left by waxing and waning of former glaciers and ice sheets during the late Quaternary has been the focus of much research. This has been hampered by the difficulty in dating such features. Luminescence has the potential to be applied to glacial sediments but requires signal resetting prior to burial in order to provide accurate ages. This paper explores the possibility that, rather than relying on light to reset the luminescence signal, glacial processes underneath ice might cause resetting. Experiments were conducted on a ring-shear machine set up to replicate subglacial conditions and simulate the shearing that can occur within subglacial sediments. Luminescence measurement at the single grain level indicates that a number (albeit small) of zero-dosed grains were produced and that these increased in abundance with distance travelled within the shearing zone. Observed changes in grain shape characteristics with increasing shear distance indicate the presence of localised high pressure grain-to-grain stresses caused by grain bridges. This appears to explain why some grains became zeroed whilst others retained their palaeodose. Based on the observed experimental trend, it is thought that localised grain stress is a viable luminescence resetting mechanism. As such relatively short shearing distances might be sufficient to reset a small proportion of the luminescence signal within subglacial sediments. Dating of previously avoided subglacial sediments may therefore be possible.

1. Introduction

As the Quaternary is typified by growth and decay of ice sheets and glaciers it is hardly surprising that much research has focussed on using geomorphology to reconstruct and model these through time (e.g., Jenson et al., 1995; Dyke et al., 2001; Clark et al., 2012; Toucanne et al., 2015; Hughes et al., 2016). Unfortunately, many of the difficulties and controversies stemming from this can be traced back to uncertainties associated with age either through problematic stratigraphic correlation or through methods attempting to provide specific ages (e.g., Hamblin et al., 2005; Pawley et al., 2008; Gibbard et al., 2009; White et al., 2010, 2016; Lee et al., 2011). Radiocarbon is of limited use as it covers only part of the last glacial-interglacial cycle, and organic preservation within glacial sediments is limited and has a high potential for carbon recycling/contamination (Briant and Bateman, 2009). Uranium series dating and amino-acid racemisation often cannot be applied through lack of suitable material within glacial sequences. As a result, Quaternary scientists largely apply cosmogenic and luminescence dating. The application of cosmogenic exposure dating, although relatively new, has been making a significant contribution to the understanding of ice-sheet fluctuations (e.g., McCormack et al., 2011; Anjar et al., 2014; Davis et al., 2015). However, exposure dating is largely limited to glacially eroded boulders on, for example, moraines and crag-and-tails (e.g., Livingstone et al., 2015) and is complicated by the presence of cold-based ice (Ballantyne, 2010).

Luminescence dating has potential to date events within the last two glacial-interglacial cycles (e.g., Bateman et al., 2011) and is applicable to quartz and feldspars that are almost ubiquitous within preserved glacial landforms and sediments. As such, the method is attractive for gaining glacial chronological frameworks. However, the technique relies on the fundamental premise that at some point between erosion, transport, or deposition, glacial sediment must be exposed to sunlight for a sufficient duration to remove antecedent stored luminescence. Godfrey-Smith et al. (1988) showed that for quartz the optically stimulated luminescence (OSL) signal is reduced to <1% of its original level within 10 s of sunlight exposure. It therefore might be viewed that this is not too hard a criterion to meet, and indeed, King et al. (2014, 2014) showed that sediment redistribution in proglacial settings has a number of opportunities to reset. However, many of the events/sediment requiring dating pertain to subglacial processes and associated landforms in which light exposure is unlikely (e.g., Lamothe, 1988; Rhodes and Pownall, 1994; Fuchs and Owen, 2008). As a result, age overestimation (e.g., Duller et al., 1995; Houmark-Nielsen, 2009) and

* Corresponding author.
E-mail address: m.d.bateman@sheffield.ac.uk (M.D. Bateman).
[1] Current address: Geophysical Fluid Dynamics Laboratory, NOAA/Princeton University, USA.

https://doi.org/10.1016/j.geomorph.2018.01.017
0169-555X/

ages in saturation or highly variable ages (e.g., Thrasher et al., 2009) can occur.

It has long been established that electrons trapped in defects within the crystal lattice of quartz or feldspar can also be stimulated into releasing luminescence by heat (thermoluminescence or TL) from natural or anthropogenic fires. What is less well established is a third environmental luminescence stimulation mechanism that relies on frictional effects or pressure (McKeever, 1985), which is known to cause triboluminescence or piezoluminescence. In this, as electrons recombine and give off luminescence, so the stored charge depletes, eventually leading to resetting (see Dreimanis et al., 1978; Aitken, 1985; Lamothe, 1988; Toyoda et al., 2000). Studies of sediment found in deep faults have shown that luminescence resetting does occur during earthquake events, but in such cases the ambient temperature is elevated and pressures induced by overburden as well as during movement on the fault are high (Zöller et al., 2009; Spencer et al., 2012). Subglacial temperatures and general confining pressures are much lower than this. Nonetheless, the existence of resetting at the ice-bed has been proposed (e.g., Morozov, 1968; Dreimanis et al., 1978; Lamothe, 1988). More recently, empirical work from the Haut Glacier d'Arolla, Switzerland, by Swift et al. (2011) appeared to show a lowered luminescence signal from subglacial samples when compared to supraglacial sediments. This they suggested was caused by the resetting of sediment during subglacial crushing and grinding (specifically, bedrock erosion and debris comminution).

Laboratory studies of the effects of mechanical crushing on sediment luminescence have generally failed to see an effect (e.g., Sohbati et al., 2011; Rittenour et al., 2012). However, Bateman et al. (2012) reported initial results from a ring-shear experiment in which changes to palaeodose (D_e) were monitored as shearing distance increased. This demonstrated for the first time that changes in stored palaeodose are possible when sediment was placed under a modest pressure (100 kPa) and sheared. They suggested that the average confining pressure applied within the ring-shear apparatus was insufficient alone to cause these changes. Instead, they concluded that stress induced during grain bridging (grain stacks or forced chains consisting of several aligned grains) events was important. They therefore suggested that geomechanical luminescence signal reduction may be a viable alternative mechanism for resetting (referred to as 'bleaching' when performed by light) of glacial sediments. However, the experiment on its own was not conclusive as it was hampered by low quantities of grains showing signs of resetting and high levels of palaeodose scatter. It was also impossible to discern, because of the low palaeodose (~4 Gy) of the sediment used, whether grains were being fully reset or their stored dose just depleted. Finally, the experiment was unable conclusively proved whether the observed changes in palaeodose were caused by pressure (normal stress), shear stress, or other mechanical changes such as localised recrystallization (or the causation and migration of defects within grains).

The aims of this present study were twofold. First, to test the results of Bateman et al. (2012) using an annealed gamma irradiated sample with much higher dose, increased sensitivity, and lower initial D_e scatter. It was hoped such an approach would provide the opportunity to see more effectively whether OSL signal resetting is actually taking place or just that palaeodose is being reduced. Second, using new surface texture and shape data from the Bateman et al. (2012) experiment and the new experiment to better understand the potential mechanisms causing any signal removal.

2. Experimental details

2.1. Sample preparation

The experiment of Bateman et al. (2012; experiment 1) and the new experiment (experiment 2) were based on sediment sampled from a dune field at Lodbjerg, Denmark, studied by Murray and Clemmensen (2001) and Clemmensen et al. (2009). This sediment was originally derived from local, sand-rich glacial till. Actual glacial sediment was not used because of its complex transport history (e.g., Fuchs and Owen, 2008), sometimes poor OSL sensitivity (e.g., Preusser et al., 2007), and mixed lithologies that may be associated with different luminescence properties and behaviour (Rhodes and Bailey, 1997; Rhodes, 2000). Sampling consisted of driving 50+ opaque 20-cm-diameter PVC tubes into the exposed dune face (Fig. S1). The tubes were transported to the laboratory, where the outer 2–3 cm of sand from each tube-end was discarded (thus excluding any grains that may have been exposed to light). Sand was then sieved through a 500 μm sieve to remove extraneous organic material (mostly small rootlets) and homogenised by mixing. Mineralogy was confirmed to be dominantly quartz by mineral-mapping ~100 grains using a Zeiss Sigma field emission analytical SEM equipped with an Oxford Instruments INCAWave detector. Further, laser granulometry confirmed the size distribution to be well-sorted medium sand (M_d = 295 μm, d_{10} = 197 μm, d_{50} = 319 μm, d_{90} = 543 μm).

For the new experiment (experiment 2), sediment was additionally annealed to 500 °C for 1 h to remove any naturally acquired palaeodose and to improve the quartz sensitivity to dose. The sediment was then given a 38.1 ± 1.2 Gy dose using the Cobalt^{60} gamma source at Risø, Denmark. This dose was selected to be of a similar magnitude to what would be expected for a relict glacial deposit from the Last Glacial Maximum (~21 ka). As the annealing and gamma dosing was undertaken in batches, all were thoroughly remixed prior to ring-shear experimentation.

2.2. Shearing in the ring-shear

For both experiments, sediment was loaded under dark room conditions into the Aarhus University ring-shear apparatus (Fig. 1A). The ring-shear consists of a large (sample surface of 1800 cm^2) circular shearing chamber with a trough for the sediment 120 mm wide and depth of 80 mm (see Larsen et al., 2006, for further details). It has two plates between which the shearing gap in the sample is located. Ribs 6 mm in length are attached to both plates to fix the sample, and shearing is created by rotating the lower plate at a constant velocity (Fig. 1B). A uniform normal stress is applied hydraulically to the sample through the normal-load plate, which is free to move vertically according to sample compaction or expansion during shearing. Shear stress is measured by two sensors mounted on the normal-load plate, and sediment compaction is monitored by three sensors attached to the normal-load plate at equal distances around the shearing chamber whereby average data recorded by each group of sensors are considered further. The approximate shearing zone position was determined during test runs conducted using glass beads as strain markers, which showed the zone of deformation to be around 2.5 cm thick (Fig. S3). During the shearing, the sand had a preexisting moisture content making it cohesive but not saturated.

For experiment 1, the ring shear apparatus was run at a uniform normal stress of 100 kPa and a shearing velocity of 1 mm min^{-1} (i.e. parameters that are in the range of typical conditions beneath glaciers and ice sheets; Paterson, 1994) to a distance of 1280 cm. During the experiment, sediment compaction, shear stress, and normal stress were recorded in 30 s intervals. Experiment 1 was periodically paused to allow sampling after shearing displacements of 10, 20, 40, 80, 160, 320, 640, and 1280 cm. At each pause, two opaque 20-mm-diameter tubes were inserted vertically into the sand in the middle of the shearing chamber, marked at the level of the shearing chamber sand, and then slowly pulled out and sealed. The mark was subsequently used to infer the location of the shearing zone in each sample. The space in the shearing chamber left after sampling was naturally backfilled by lateral sediment creep while the tube was removed so that the original stratification was reinstated as closely as possible. This formed the basis of the samples used for sediment and for OSL characterisation. Before

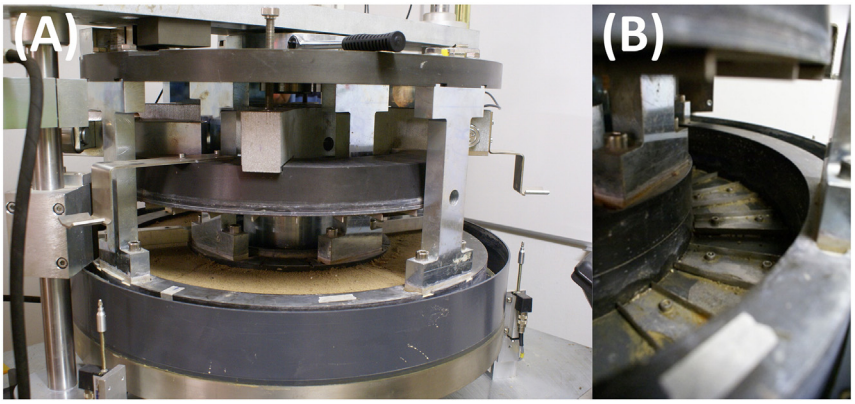

Fig. 1. The ring shear apparatus used for both experiments. (A) Apparatus loaded with sediment at end of the experiments. (B) The empty ring shear chamber showing the ribs on lid (top of picture) and in the base of the trough used to create shear stress.

the start of the shearing and after each sampling, the sediment was consolidated under the normal stress of 100 kPa. Experiment 2 was run with the same parameters as above except that after shearing displacement of 1280 cm, normal stress was increased to 150 kPa and velocity to 2 mm min^{-1} and a final sample was collected after a total shearing displacement of 1920 cm.

2.3. Luminescence measurements

All OSL sample preparation and analyses of samples from experiment 2 were carried out in the University of Sheffield luminescence laboratory under controlled lighting conditions. For each ring-shear sample, subsamples were taken by cutting 1-cm sections of tube with a pipe-cutting tool. This avoided any mechanical damage to grains that sawing would have caused. The position of the shearing zone was determined based on a prior test experiment using glass beads as strain markers that showed a 2.5-cm-thick shearing zone located in the middle of the sample tube (see Supplementary information for more details). Two sets of subsamples were collected: (i) from 1 cm below the shearing zone (referred to herein as unsheared), and (ii) centred on the shearing zone (referred to herein as sheared). The former samples were taken for the purpose of investigating the effects of pressure alone and the latter for the combined effects of shear stress and pressure.

The OSL measurements focussed on quartz rather than feldspar as quartz dominanted in terms of grain numbers within these small samples and feldspar grains have potential anomalous fading issues. The quartz from all subsamples was extracted and cleaned for OSL dating (see Bateman and Catt, 1996, for details). Given the limited sample size, prepared quartz between 90 and 250 μm dimeter was used. Single grain OSL measurements were made on a TL-DA-15 Risø reader with a green laser single grain attachment (Duller et al., 1999). In principle, with the grain size used, more than one grain could have been mounted in the 300 μm Risø grain holder and measured simultaneously. However, given that <10% of grains were smaller than 197 μm and that most grains emitted insufficient OSL, the chances of more than one grain contributing to a stored dose (D_e) was considered extremely low. Luminescence was filtered with a 2.5-mm-thick Hoya U-340 filter (as per Ballarini et al., 2005) and irradiation was provided by a calibrated $^{90}Sr/^{90}Y$ beta source. The OSL stimulation was for 0.8-s, whilst the sample was held at 125 °C. The D_e values within grains were measured using a single aliquot regeneration (SAR) protocol with a 10-s, 260 °C preheat experimentally determined from a dose recovery preheat plateau test (Murray and Wintle, 2003). The SAR growth curves for each grain were based on an integral of OSL measured between 0.08 and 0.11 s and background on an integral of OSL measured between 0.64 and 0.8 s. When analysing the SAR data, grains were only accepted where the recycling ratio was 1 ± 0.2 of unity; recuperation was <5%; the error on the test dose was <20%; the naturally acquired OSL was significantly above background; and SAR regeneration points could be fitted by a growth curve. To demonstrate the appropriateness of this measurement protocol, dose recovery tests were undertaken with two samples (Shfd12089 and Shfd12090), which both returned measured palaeodoses within unity of those given (1.03 ± 0.03 and 1.02 ± 0.03 respectively), low overdispersion (7% and 5%), and normal D_e distributions (Fig. S5). Importantly, given the subsequent results from the ring-shear experiment samples, no zero-dose grains were measured during these dose recovery tests.

The natural sediment used in Bateman et al. (2012) required 3000–5000 grains to be measured per sample to meet a minimum of 35 accepted grains. Annealing clearly improved the sediment sensitivity as only between 400 and 1300 grains per sample needed to be measured for a minimum of 50 D_e values to meet the acceptance criteria (Rodnight, 2008). Data shown in Tables 1 and 2 represent the measurement of over 21,000 grains. As it was key to find potentially small numbers of reset (i.e. zero-dose) grains and grains with depleted D_e values, two subsamples (see samples Shfd12089 and Shfd12090 in Table 1) were measured independently three times to evaluate the reproducibility of results. For the purposes of this experiment, zero-dose grains were defined as those with D_e values within uncertainty of 0 Gy and their numbers were recorded as a percentage of the accepted grains. Results were analysed using the central age model (CAM; Roberts et al., 1999), which also allowed calculation of overdispersion (OD; percentage of uncertainty greater than can be explained by the errors calculated around the central value). As the data sets were non-normally distributed results were also analysed with the finite mixture model (FMM; Galbraith and Green, 1990) where a σb value of 0.20 was used (as per Livingstone et al., 2015) and k was selected to minimize the Bayesian information criterion (BIC) value.

2.4. Sediment characterisation measurements

Changes in grain shape were quantified at first manually (experiment 1) and then using automated image-based methods (experiments 1 and 2). Manual analysis was performed by visual Bateman classification of grains viewed under a microscope using Power's roundness index (Powers, 1953). Automated analysis was used to measure specific grain attributes (including particle area, perimeter length, Feret, and breadth) that enable calculation of common shape parameters (Table 3). First, optical or SEM images of 50 randomly selected grains per subsample were analysed using the 'Gold Morph' shape-analysis plug-in (Crawford and Mortensen, 2009) for the ImageJ image processing and analysis software programme (imagej.nih.gov/ij/). Second, the remaining material was analysed using a Sympatec QICPIC Image Analyser system fitted with a 532-nm laser and a high-speed

Table 1
OSL single grain data from shearing experiment; results for the sheared and unsheared samples.

Labcode	Shearing distance (cm)	No. grains measured	No. grains accepted	Central age modelling		Finite mixture modelling				D_e distribution characteristics		
				Mean	OD	Dominant component		Other component		Zero grains	Skew	Sort
				D_e (Gy)	(%)	D_e (Gy)	Prop (%)	D_e (Gy)	Prop (%)	N (%)[a]		
Unsheared												
Shfd11227	0	1200	75	37.0 ± 1.5	32	44.6 ± 2.5	62	27.4 ± 2.0	38	0 (0)	1.37	0.31
Shfd11218	10	1200	64	40.0 ± 1.8	35	41.2 ± 1.5	90			0 (0)	4.91	0.23
Shfd11219	20	1100	73	38.8 ± 1.8	37	40.2 ± 1.4	83	23.4 ± 2.6	15	0 (0)	2.84	0.28
Shfd11220	40	1200	64	38.4 ± 1.4	26	36.7 ± 1.2	94			0 (0)	1.41	0.26
Shfd11221	80	1200	79	34.9 ± 1.1	25	36.3 ± 1.3	93			0 (0)	0.24	0.25
Shfd12091	160	400	49	36.1 ± 2.1	37	36.3 ± 1.7	81	19.9 ± 3.3	11	0 (0)	0.88	0.41
Shfd11223	320	900	67	36.1 ± 1.5	31	37.1 ± 1.0	98			0 (0)	0.46	0.25
Shfd11224	640	1000	61	36.9 ± 1.0	17	36.9 ± 1.0	100			0 (0)	0.22	0.19
Shfd12094	1280	900	80	38.2 ± 1.4	31	35.6 ± 1.6	88	66.0 ± 14.8	12	0 (0)	1.29	0.30
Shfd11226	1920	1200	59	36.5 ± 2.0	40	36.8 ± 1.29	92			0 (0)	2.16	0.29
Sheared												
Shfd12087	10	500	63	38.6 ± 1.5	29	40.8 ± 1.7	91			0 (0)	0.25	0.31
Shfd12088	20	600	69	39.5 ± 1.3	25	37.3 ± 1.4	88			0 (0)	0.68	0.27
Shfd12089	40	700	74	40.9 ± 1.3	21	41.5 ± 1.1	98			0 (0)	0.42	0.32
Shfd12090	80	600	59	38.8 ± 1.2	23	40.4 ± 1.1	98			0 (0)	0.93	0.39
Shfd11222	160	1300	71	35.4 ± 1.4	30	39.1 ± 1.7	82	22.4 ± 3.1	18	2 (2.8)	1.06	0.35
Shfd12092	320	600	73	36.8 ± 1.5	32	39.3 ± 1.4	92			1 (1.4)	0.48	0.30
Shfd12093	640	800	80	37.7 ± 1.3	28	39.0 ± 1.2	96			1 (1.3)	0.48	0.28
Shfd11225	1280	1100	66	35.8 ± 1.5	30	37.6 ± 1.2	95			2 (3)	0.39	0.27
Shfd12095	1920	700	80	43.3 ± 1.7	31	49.7 ± 2.62	73	29.4 ± 3.3	27	8 (10)	0.49	0.47

[a] Absolute number of zero-dose grains. In parenthesis, percentage of zero-dose grains as a function of total grains that gave D_e values meeting the quality assurance criteria.

Table 2
OSL single grain data from replicated samples from shearing experiment; the given initial gamma dose was 38.1 ± 1.2 Gy.

Labcode	No. grains measured	No. grains accepted	Central age modelling		Finite mixture modelling				D_e distribution characteristics	
			Mean	OD	Dominant component		Other component		Skew	Sort
			D_e (Gy)	(%)	D_e (Gy)	Prop. (%)	D_e (Gy)	Prop. (%)		
Shfd12089(1)	700	74	43.6 ± 1.6	27	46.8 ± 2.0	85	28.3 ± 4.30	15	0.42	0.32
Shfd12089 (2)	300	47	40.6 ± 1.5	22					0.59	0.23
Shfd12089 (3)	700	53	40.9 ± 1.3	21	41.5 ± 1.3	98			0.11	0.21
Shfd12090 (1)	600	59	38.9 ± 1.9	33	32.4 ± 2.1	65	54.9 ± 5.8	35	0.93	0.39
Shfd12090 (2)	600	72	38.0 ± 1.3	28	43.6 ± 2.1	69	27.7 ± 2.3	31	0.21	0.28
Shfd12090 (3)	800	69	39.8 ± 1.2	23	40.4 ± 1.1	98			0.45	0.24

(70 Hz s^{-1}) CMOS camera, which permitted analysis of 19,000+ particles per sample.

Calculated shape parameters are shown in Tables 3 and 4 (parameter variables are defined in Table 5). Parameters for optical and SEM image analysis (Table 3) were selected for their sensitivity to changes in grain shape as illustrated by the accompanying diagrams to Krumbein's (1941) scale of roundness (shown in modified form in Fig. S2). Parameters in Table 4 are calculated automatically by the QICPIC analysis software. Two of these (*Sphericity* and *Convexity*) have direct equivalents in Table 3 (although their outputs are inverted), whilst *Aspect Ratio* has some equivalency to *Round* (Table 3) because these parameters relate either longest or shortest length to particle area. All such parameters are limited in that they allow characterisation of overall particle form only, whereas the Krumbein and Power's Roundness indexes require the user to classify particles based on a combination of overall form (e.g., their *blockyness*) and individual edge characteristics (e.g., the 'sharpness' of their asperities). However, because edge characteristics (including fractures) do contribute to overall form of small particles, these more quantitative approaches should offer significant advantages over manual (e.g., Power's) techniques. The QICPIC

Table 3
Shape parameters used to interpret quantitative particle morphology data obtained by ImageJ analysis of Krumbein plots and optical and SEM images of shearing experiment sediment.

Parameter	Example use or source	Formula	Comment	Krumbein scale comparison[a]
Circ	Roussillon et al. (2009)	$\frac{P_s}{2\sqrt{A_s\pi}}$	Compares perimeter of particle with that of 2D disk of same area. Influenced by elongate particles that deviate from spheroid shape.	+ve (↑*Circ* value)
rP	Roussillon et al. (2009)	$\frac{P_s}{P_e}$	Use of perimeter of ellipse intended to remove influence of particle elongation when attempting to capture roundness.	+ve (↑*rP* value)
Conv	Roussillon et al. (2009)	$\frac{A_s}{A_{CH}}$	Convex hull fitted to particle (rather than ellipse) further removes influence of elongation when attempting to capture roundness.	−ve (↓*Conv* value)
Conv2	Cox and Budhu (2007)	$\frac{P_{CH}}{P_s}$	As Conv (above) but uses particle perimeter and convex hull perimeter rather than area.	−ve (↓*Conv2* value)
Round	Cox and Budhu (2007)	$\frac{4A_s}{\pi L^2_{Feret}}$	Relates area to longest length. Sensitive to evolution of 'sharp', elongated forms.	−ve (↓*Round* value)

[a] Regression using reversed Krumbein (1941) scale (Fig. S1). All relationships significant at $p < 0.001$.

Table 4
Shape parameters calculated by the QICPIC analysis software (https://www.sympatec.com/EN/ImageAnalysis/Fundamentals.html); for details on terms within the formulas see Table S1.

Parameter	Formula	Comment	Interpretation
Sphericity	$\frac{2\sqrt{A_s\pi}}{P_s}$	Circularity in for a 2D shape. Identical to inverse of *Circ* (Table S1). Influenced by particle elongation.	↑angularity = ↓*Sphericity*
Aspect Ratio	$\frac{L_{min}}{L_{Feret}}$	Ratio of shortest to longest axis. Measures particle elongation (similar to ratio of B-axis to A-axis).	↑ angularity = ↓*Aspect Ratio*
Convexity	$\frac{A_s}{A_{CH}}$	Identical to *Conv* (Table S1). Convex hull fitted to particle eliminates influence of elongation.	↑angularity = ↓*Convexity*

parameters are by default calculated for grains in specific size ranges, meaning, for simplicity, individual size-category values were combined into a single mean value.

In addition to the above, at the end of experiment 1 a vertical thin section oriented parallel to the shearing direction along the middle of the sample was prepared from an undisturbed sediment block. This was to permit examination of grain arrangement and characteristics in situ (i.e. within the shearing zone). The thin section was subdivided into 18 equally thick segments and in each of them, the orientation of elongated grains was determined separately. On average, 32 grains with axial ratios of at least 2:1 per segment were measured. The orientations are expressed as S_1 eigenvalues (Mark, 1973) and as main dip angles (MDA) representing the averaged angle of dip of the 18°-wide sector of rose diagram that contains the highest number of single measurements.

3. Results

3.1. Luminescence

Luminescence results for experiment 1 were presented in Bateman et al. (2012) so only the new results for experiment 2 are outlined here. For the unsheared subsamples, with progressive shearing the mean D_e (based on CAM) shows a slight decrease after 80 cm, but with an r^2 of only 0.02 this is not significant (Fig. 2A). For sheared samples, the mean D_e shows a slight decrease after 320 cm, but with an r^2 of only 0.08 again this is not significant especially if the final point is excluded on the basis that it was sheared at a high normal stress (150 not 100 kPa; Fig. 2B). All samples showed a surprising level of OD that was on average 30% (Table 1) and did not increase with shearing distance. Looking at the FMM results, both sets of subsamples show weak trends toward decreasing D_e with shearing distance (Fig. 3). The r^2 values are higher than the CAM (0.2 and 0.4 respectively) reflecting FMM isolating some small (<10% of the data) components for some samples. The latter may reflect a small number of measurements where more than one grain was measured simultaneously. Zero-dose values through necessity had to be excluded from the logarithm-based FMM analysis.

More than one FMM component was found with some sheared and unsheared subsamples, but this is not a systematic effect. To check this, two randomly selected samples were run independently three times to establish internal variability in the mean and component D_e values (Table 2). Sample Shfd15090 returned CAM D_e values within errors but one replicate had only one FMM component compared to the two components of the other two replicates. For sample Shfd15089, one replicate returned two FMM components compared to the one component identified for the other two replicates. Additionally, one of the replicates failed to return a CAM D_e within errors of the other two replicates. In the light of the variability of the replicate data, and despite using a σb value three times higher than the OD established with the dose recovery experiments (5–7% measured, 20% applied) and minimising the BIC, FMM failed to accurately fit to and extract components from these data, and the results are therefore unreliable.

The critical luminescence data appear to be the number of zero-dose grains measured. No zero-grains were found in the 10 samples (>10,000 grains measured) taken from the unsheared zone regardless of the shearing distance travelled. Further, no zero-grains were measured on the sheared material during the two dose-recovery experiments undertaken (1600 grains measured, Fig. S5). Zero-grains appeared only within the shearing zone after the shearing distance exceeded 100 cm (after 2400 grains from shorter distances had already been measured). As shown in Fig. 4, as a function of total grains that met the quality acceptance criteria, zero-dose grains remained low (max. 8 grains out of 80 grains in sample Shfd12095) but linearly increased with shear distance ($r^2 = 0.8$; note logarithmic distance scale in Fig. 4). Whilst the number of zero-dose grains was small, this is the second separate experiment that has generated them (the first being that of Bateman et al., 2012). Further measurements for longer distances could not be undertaken because of constraints on machine time (ring-shear experiment 2 took over 13 days to run excluding stops to permit sampling) and because at longer distances multiple rotations of the circular ring-shear machine increased the possibility of collecting sediment already disturbed by earlier sampling.

3.2. Sediment characterisation

Results demonstrated that, despite an initial degree of angularity and fracture presence, experiment 1 sheared zone subsamples exhibited increasing angularity and elongation with shearing distance (e.g., Fig. 5, Table 6), confirmed by Power's roundness and fracture incidence (Table 7). Most notably, analysis of SEM grain images demonstrated observable correlation with shearing distance (here defined as $p \le 0.1$) for parameters *Conv2* and *Round*, weakly observable correlations ($p \le 0.35$) for parameters *rP* and *Conv*, and a significant correlation ($p \le 0.05$) for the parameter *Circ* (Figs. 5 and 6; Table 6). This was supported by QICPIC analysis, which demonstrated a significant correlation with shearing distance ($p \le 0.05$) for *Convexity* (Table 6). Interestingly, QICPIC size results (Table 5) also demonstrated a statistically significant correlation between particle size and shearing distance, demonstrating an increase in sediment size within the shearing zone (Fig. 7).

Experiment 2 shearing zone subsamples are not entirely consistent with those for experiment 1, demonstrating some inconsistent parameter changes, including a decrease in the *Circ* parameter and particle diameter, an increase in the *Conv2* and *Sphericity* parameters, and no apparent decrease in the *Conv* and *Round* parameters (Table 6). Some parameter changes consistent with experiment 1 were instead observed in unsheared subsamples, specifically for *Circ*, *Conv*, *Round*, *Convexity*, and *Aspect Ratio*, together with a weakly observable increase in particle size (Table 6); although *Sphericity* was again observed to increase. Manual analysis did nonetheless demonstrate some change in Power's roundness and fracture incidence for sheared zone

Table 5
Shape formula variables (Tables 3 and 4).

Variable	Description
P_s	Perimeter of the particle silhouette
P_e	Perimeter of the smallest ellipse that encloses the particle silhouette
A_s	Area enclosed by the particle silhouette
P_{CH}	Perimeter of the smallest convex hull that encloses the particle silhouette
A_{CH}	Area of the smallest convex hull that encloses the particle silhouette
L_{Feret}	Length of the particle's Feret diameter
L_{min}	Length of the particle's shortest axis

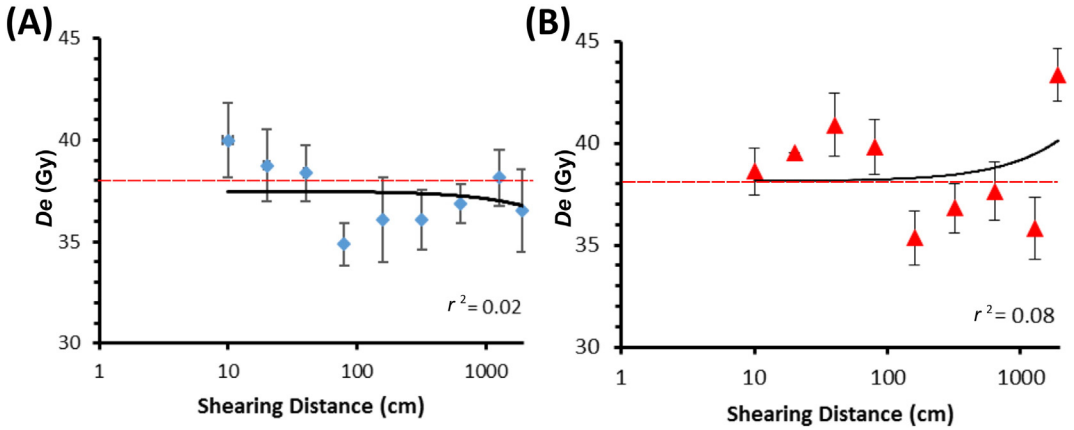

Fig. 2. CAM D_e values from (A) unsheared and (B) sheared samples with distance sheared. Dashed red line shows the initial gamma dose value. Note final point underwent shearing at an extra 50 kPa.

subsamples and failed to show any observable changes for unsheared samples (Table 7). These less clear-cut results for experiment 2 appear to indicate that the shearing zone constituted a wider, more diffuse zone than observed during experiment 1.

Thin section results from experiment 1 demonstrated that S_1 values, which express the orientation strength of elongated grains, were between ~0.42 and ~0.76 and grains typically exhibited low-angle dips (Figs. 8 and 9). There was no clear pattern in the orientation strength within the shearing chamber, but two peaks are visible (Fig. 8). The peak of S_1 values in the middle of the shearing zone is attributed to grain advection and rotation toward quasi-stable positions with grain long axes oriented parallel to the shearing direction (Hooyer et al., 2008). The second peak at the top of the deposit, well above the shearing zone, is possibly caused by repeated compaction that the deposit has been subjected to at the start of each shearing increment. There is no systematic downflow or upflow dip direction of elongated grains within the shearing zone.

3.3. Ring shear monitoring data

Parameters recorded during experiment 2 are shown in Fig. 10. During this experiment, the prescribed normal stress (100 or 150 kPa) varied by $<\pm 0.12$ kPa, which is negligible. The total compaction of the sediment at the end of experiment reached about 6 mm reflecting a combination of pore space reduction because of denser grain packing and grain-size reduction due to grain abrasion and fracturing. However, some apparent compaction also occurred as a result of sediment being squeezed out of the chamber through the shearing gap (although not measurable the volume was estimated as <1% in relation to the overall sediment volume in the chamber). The highest compaction rates were achieved at the beginning of the shearing whereby half of the total compaction (~3 mm) occurred during the initial shearing displacement of ~5 cm. After about 170 cm of shearing, compaction became approximately linear and small and increased slightly again during the last shearing increment under increased normal stress of 150 kPa. Despite the granular character of the material, no dilatant volume increase at the beginning of shearing was noticed, possibly because of the fine-grained nature of the sand. The average shear stress generated in the deforming material was ~36 kPa during the shearing under normal stress of 100 kPa and ~55 kPa under normal stress of 150 kPa. During the entirety of experiment 2, shear stresses fluctuated significantly with an amplitude of up to ~18 kPa. Stress variations of several kPa occurred over shearing displacements of just a few centimeters (Fig. 10). After a shearing displacement of about 800 cm certain cyclicity in stress fluctuations with a wavelength of around 60 cm became apparent. This was possibly caused by recurrent grain-rearrangement events that become predictable after a quasi-steady state of deformation has been reached. During shearing under normal stress of 100 kPa, the magnitude of stress variations increased toward the end of the experiment and remained high during shearing under normal stress of 150 kPa.

4. Discussion

The marker displacement of shearing chamber sediments reported in Bateman et al. (2012) indicated that shearing took place within a

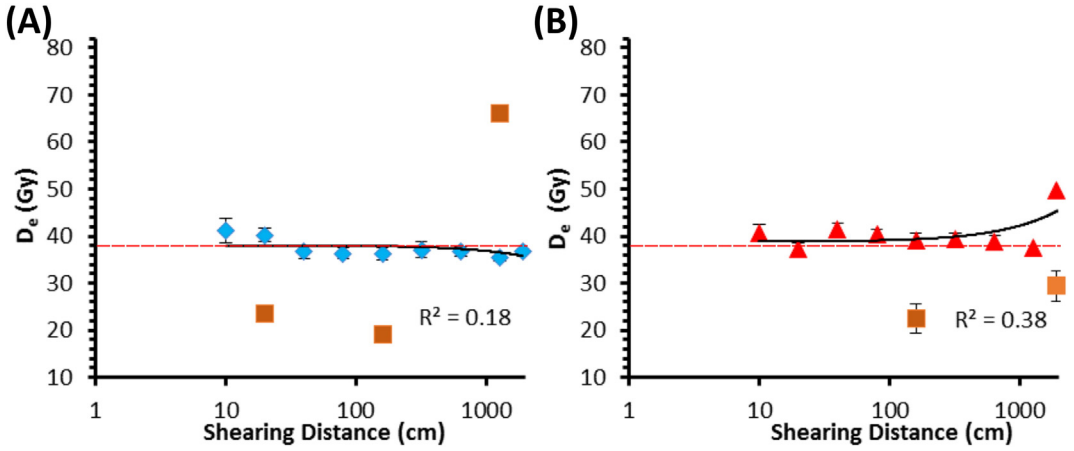

Fig. 3. FMM D_e component values (those representing >10% of data only) from (A) unsheared and (B) sheared samples with distance sheared. Blue/red indicates dominant component and brown other components extracted. Dashed red line shows the initial gamma dose value. Note final point underwent shearing at an extra 50 kPa.

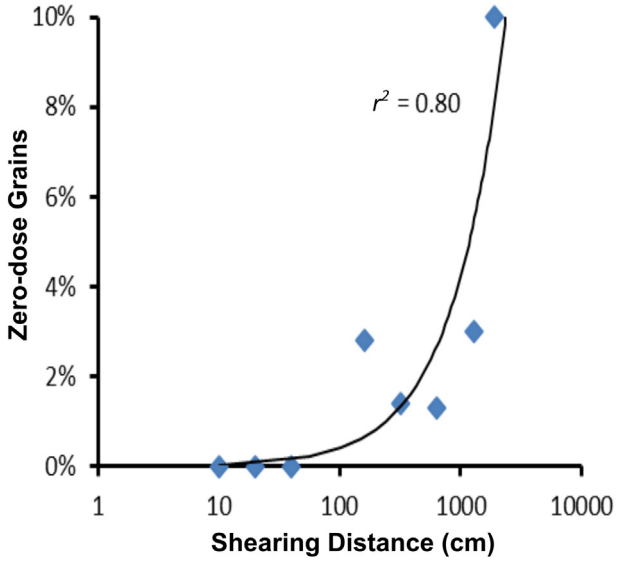

Fig. 4. Zero-dosed grains measured as a proportion of total number of grains accepted. Note final point underwent shearing at an extra 50 kPa.

narrow, well-defined shearing zone. This is supported by sediment characterisation of the sheared subsamples from experiment 1 that indicated the evolution of particle shape toward more angular and elongated morphologies. This is consistent with fracturing of grain surfaces as a result of grain-grain stresses imposed during sediment deformation and an increase in apparent average grain size. Thin section results also indicate the development of alignment of larger grains in the shearing zone. It is proposed that the apparent grain size increase and alignment observations result from the rotation of larger grain in the shearing zone causing smaller grains to be expelled from it. As a result of the cohesive nature of the sediment and lack of free-water, it is possible that grains were expelled in both directions.

Mixed observations of size and shape changes for both sheared and unsheared subsamples from experiment 2 indicate that the shearing zone may have occurred in a wider zone than for experiment 1. It may be possible to disregard the inconsistent *Circ*, *Conv2*, and *Sphericity* parameter changes observed for sheared zone samples. *Circ* and *Sphericity* (Tables 3 and 4) relate particle perimeter length to that of an idealised sphere of the same area, which is unlikely to apply to initially nonspherical geological particles. *Conv2* (Table 3) uses perimeter length to calculate convexity and is therefore likely to capture changes in surface roughness rather than overall form. However, the statistically significant decrease in grain size shown by the sheared samples, which is inconsistent with experiment 1, remains. Irrespective of this, grains in the sheared and unsheared subsamples might be expected to have experienced high stresses and mechanical fracture.

Based on the luminescence results in this current experiment we can confirm some of the preliminary findings reported in Bateman et al. (2012). In the latter, they reported that shearing led to changes in D_e distributions with grains displaying increases and decreases in D_e including some zero-dosed grains. It was hoped that in experiment 2, with a much higher stored dose, with shearing distance there would be more grains with a reduced (but not zeroed) D_e relative to the given dose. This was not observed because, whilst sheared and unsheared subsamples returned individual grain D_e values higher and lower than the given gamma dose, neither sets showed significant trend with distance sheared. Experiment 2 did nonetheless confirm the increase in zero-dose grains observed by Bateman et al. (2012) (their Fig. 4) with the occurrence of a small number of zero-dose grains increasing with shearing distance but only for sheared sediment grains.

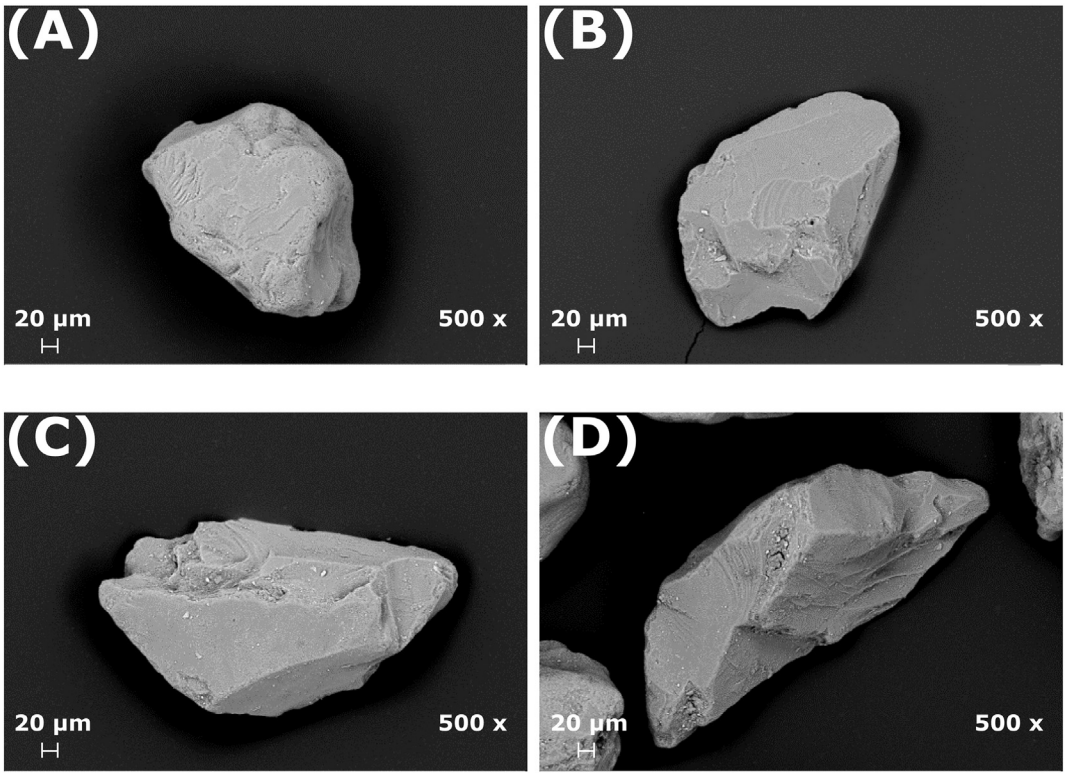

Fig. 5. SEM images of particles from subsamples of unsheared material (above) and sheared material (below) (experiment 1). Unsheared material contains some angular and fractured particles, but many fractures do not appear fresh (e.g., top left) or recent fractures are few in number and asperities typically remain well rounded (e.g., top right). Sheared material contains a larger number of particles with an apparently greater fracture incidence and dominantly angular and sharp asperities (bottom images). Nonetheless, a large proportion of particles in all samples do not show any evidence of fracture, indicating that grain-grain stresses during shearing are highly heterogeneous.

Table 6
Trend and statistical significance of changes in particle shape and size during shearing; regression was undertaken on log-transformed shearing distance values for all analyses.

Experiment/Zone	Optical and SEM image					QICPIC analysis			Particle diameter analysis	
	Circ	*rP*	*Conv*	*Conv2*	*Round*	*Sphericity*	*Convexity*	*Aspect ratio*	Surface mean diameter	Volumetric mean diameter
Krumbein	↑↑↑	↑↑↑	↓↓↓	↓↓↓	↓↓↓	n/a	n/a	n/a	n/a	n/a
Experiment 1/sheared	↑↑↑	↑	↓	↓↓	↓↓	-	↑↑↑	-	↑↑↑	↑↑↑
Experiment 2/sheared	↓↓	↑↑↑	-	↑↑↑	-	↑↑↑	↑↑↑	↑	↓↓↓	↓↓↓
Experiment 2/unsheared	↑↑	-	↓↓	-	↓↓	↑	↑↑↑	↑↑↑	↑	↑

Key: ↑↑↑ $p \leq 0.05$; ↑↑ $p \leq 0.1$; ↑ $p \leq 0.35$; ↑ positive and ↓ negative correlation; - indicates $p > 0.35$.

Taken together it would appear that grains apparently have a bimodal response, either completely retaining their dose or completely losing it during shearing.

This leads to the question as to what within the shearing process could be the cause of a minority of grains to be reset whilst other grains are unaffected. Possible mechanisms include grain fracture, which is postulated to reduce the number of active luminescence centres that are surrounded by an extended atomic lattice (Toyoda et al., 2000), the ejection of trapped electrons by stresses imposed on the crystal lattice (Lee and Schwarcz, 1994), localised frictional heating at grain boundaries (Fukuchi, 1989; Lee and Schwarcz, 1994), and wear of grain surfaces leading to loss of alpha-induced luminescence stored near grain surfaces (Lamothe, 1988; Takeuchi et al., 2006). The results of this study indicate that grain fracture is unlikely because grain size observations appear to support smaller grains being expelled from the shearing zone rather than this zone comprising particles that have been cleaved. Further, sand-sized quartz grains formed by the comminution of larger clasts beneath glaciers are thought to be highly resistant to further fracture (Wright, 1995), indicating that observations of changes in grain size may result largely from sorting, as opposed to cleavage. This is supported by observed grain shape changes being relatively modest, with fracturing acting only to modify grain faces and edges.

Frictional heating at grain boundaries or wear to grain surfaces (e.g., Lamothe, 1988) is easily excluded mainly because it would be localised at grain surfaces, such that any effect on luminescence will have been removed by the HF acid etching during sample preparation. Additionally, the use of a laser to stimulate grains during OSL measurement should ensure rapid depletion of all optical traps throughout translucent quartz grains. If heterogeneity existed in trap defects within the crystal lattice and only traps *near* the grain surface (but sufficiently deep they survive etching) were storing dose, then the mechanical surface removal observed could potentially lead to resetting. However, two arguments can be put forward against this. Firstly, mechanical alteration appears to be related to shearing distance and so the amount of surface removed from a grain could be expected to increase with distance. That being the case, we would expect to see a rapid initial reduction in grain D_e as a result of the *high dose* grain surface being removed first, then a slower reduction associated with the exposure of the *low dose* core. The OSL data from both experiments do not detect initial D_e reduction only an increase in zero-doses. Secondly, some mechanical alteration (Table 5) is also detected in the below shearing zone subsamples, for which no zero-dose grains were observed. Thus, the reduction to zero-doses measured in experiments 1 and 2 could not just be occurring at grain surfaces, and the removal of some grain surfaces during shearing apparently is not removing palaeodose for most grains.

Application of stress, on the other hand, might affect defects in the crystal lattice such that localised recombination of electrons could occur giving rise to triboluminescence (Lee and Schwarcz, 1994) and lowering the overall dose within a grain. As the concentration of trapped charge and the number of photons produced are low, this would seem unlikely. Alternatively, elevated stress on the crystal lattice (and possibly associated temperature from friction; Fukuchi, 1989; Lee and Schwarcz, 1994) could cause the redistribution of trapped charge into more unstable traps thereby leading to apparent resetting when samples were measured months later. Simple laboratory grinding of sediment with a pestle and mortar has been observed to reduce and increase measured D_e through charge redistribution and/or triboluminescence (Phil Toms, Gloucester University, pers. com.). Charge redistribution is supported by Bateman et al. (2012) who observed a decrease with shearing of the stable 375 °C TL peak with a corresponding increase in signal in the less stable 240 °C peak. Nonetheless, establishing this as a mechanism requires further work. For example, it would be necessary to investigate the effect on the signal caused by the orientation of the crystal structure relative to the maximum stress imposed by grain bridges.

It is clear in comparing the sheared and unsheared subsample sets that alterations to palaeodose are not occurring simply as a result of general pressure (i.e. the normal stress) exerted on the sediments (100 kPa). Had this been the case, zero-dosed grains would have been observed from unsheared samples. Apparent resetting of the whole grain is concordant with elevated stresses (over and above the pressure applied to all sediment) imposed on grain crystal lattices during shearing. Shear stresses and the resulting strain distribution in granular materials are well known to be highly heterogeneous (e.g., Drescher and de Josselin de Jong, 1972; Iverson et al., 1996; Li and Aydin, 2010) and that the deforming material develops domains of different mechanical behaviour with sizes across several orders of magnitude between millimetres (micromorphology) and kilometres (macrotectronics) (Mandl et al., 1977). Experimental laboratory work has demonstrated that uneven strain distribution results in the formation of discrete shear planes that focus sediment advection whereas grains between the shear planes either remain largely stable or undergo rotational movement (cf. Damsgaard et al., 2013) leading to sediment 'skeleton' evolution (e.g., Larsen et al., 2006, 2007; Narloch et al., 2012, 2015; Menzies et al., 2013). The latter may generate grain bridges that support stresses up to several times (Iverson et al., 1996) or even an order of magnitude (Mandl et al., 1977) greater than the general stress in the surrounding material. Grain bridges fail by fracture of the particles, slip between the particles in the bridge, frictional slip between the outermost particles in the bridge and the surface of blocks sliding above and below, and by wear (abrasion) of the particles (Biegel et al., 1989; Hooke and Iverson, 1995), all resulting in spontaneous rearrangements of the skeleton and stress relief.

As stated earlier, strong evidence exists of pronounced stress heterogeneity during shearing experiment 2, especially in its second half, when normal pressure was 150 kPa and induced shear stress varied

Table 7
Trend and statistical significance of changes in particle shape and size during shearing measured from optical, SEM and QICPIC image analysis (see text). All regressions were undertaken on log-transformed shearing distance values.

Experiment/zone	R	%Frac	%R	%A	%VA
Experiment 1/sheared	↓↓↓	↑↑↑	↓↓↓	↑↑↑	–
Experiment 2/sheared	↓↓↓	↑↑	↓↓	↑↑↑	↑↑
Experiment 2/unsheared	–	–	–	–	–

Key: ↑↑↑ $p \leq 0.05$; ↑↑ $p \leq 0.1$; ↑ positive and ↓ negative correlation; — indicates $p > 0.1$.

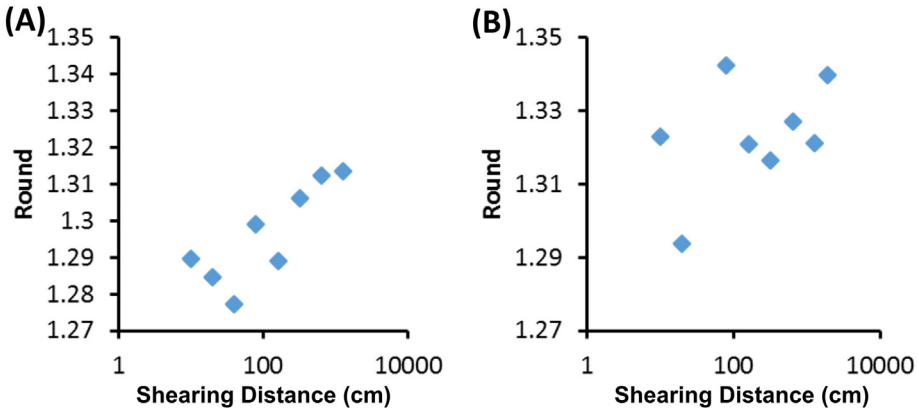

Fig. 6. Evolution of *round* (calculated on area of longest length; see Supplementary information for further details) in shearing-zone subsamples from (A) experiment 1 of Bateman et al. (2012) and (B) experiment 2.

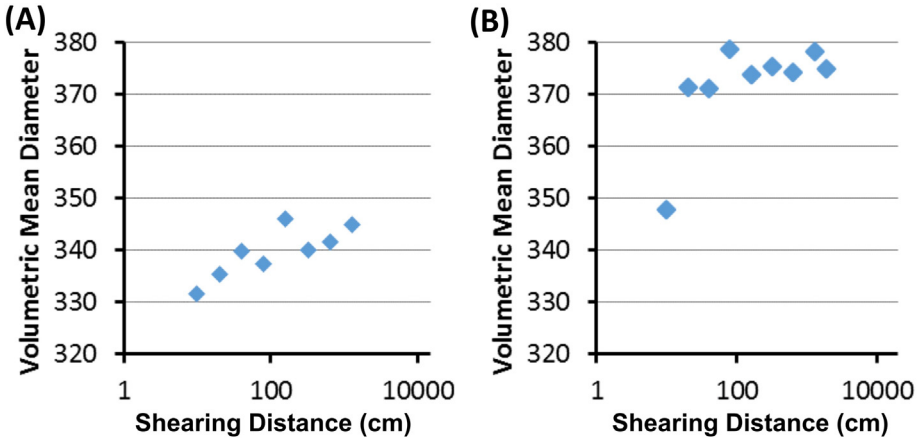

Fig. 7. Evolution of size in sheared subsamples from (A) experiment 1 and (B) experiment 2. Note the offset between experiments 1 and 2 attributed to inadvertent sorting during subsampling for artificial dosing.

from 47 up to 65 kPa. Notably, these recorded stress values are an average value resulting from multiple local stress events in the sample, and therefore the amplitude of grain-to-grain stresses at the scale of grain

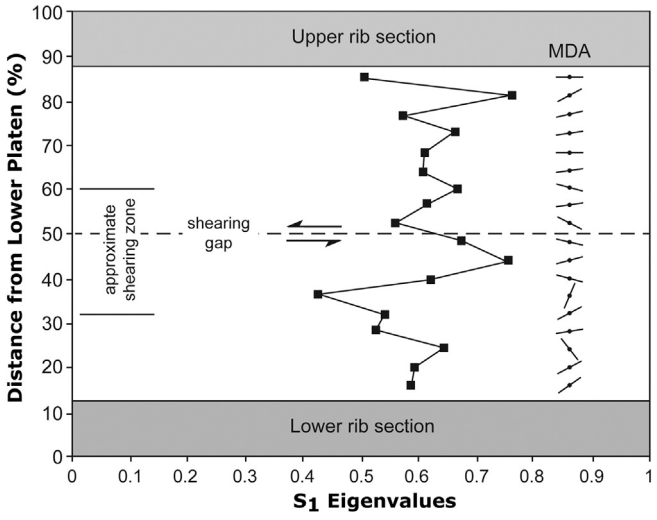

Fig. 8. Vertical distribution of S_1 eigenvalues in the sediment at the end of experiment 1 after a shearing distance of 1280 cm. Note the relatively high eigenvalues in the shearing zone. Also shown is the distribution of main dip angles (MDA) of elongated grains at each depth, whereby a horizontal line is 0° dip and a vertical line is 90° dip.

bridges and local shear planes must have been significantly greater. Brittle deformation of quartz grains has been observed at 200 Mpa (Bisschop et al., 2005) and 7000 kPa with a strain rate around 10^{-12} s^{-1} (Gueydan et al., 2005). It is unlikely these sorts of pressures occurred at the grain-to-grain level. However, if the work of Mandl et al. (1977) is correct, pressures within bridges could have reached up to 650 kPa whilst others have suggested it could exceed 5000 kPa (Boulton, 1974; Cohen et al., 2005). As grains move from spheroids to more angular forms, as shown by the sediment data, so the potential for more uneven grain packing leading to more frequent bridge-building events and more extreme stresses during these events should increase. The increase in zero-dose grains with distance should therefore mirror changes in grain shape and more variability in monitored stress data, which it does. Thus, some more angular grains within highly stressed bridges could have had their D_e depleted, whereas other grains could have avoided this by being located in more sheltered areas between the shear planes and grain bridges. The net effect of this is the uneven yet distinct increase in numbers of zero-dose grains in the shearing zone with increasing shearing displacement (Fig. 4).

Zero-dose grains have been measured from nonglacial environments. Some can be attributed to post-depositional disturbance leading to grains moving to the surface, being reset and then being reburied (e.g., Bateman et al., 2003, 2007). This is clearly not the case for this experiment or for most glacial landforms. Other causes of zero-dose grains may be attributable to poor quartz characteristics (e.g., Preusser et al., 2007), which has hampered dating of glacial sediment (e.g., in the Swiss Alps) or measurement issues. The experiment presented

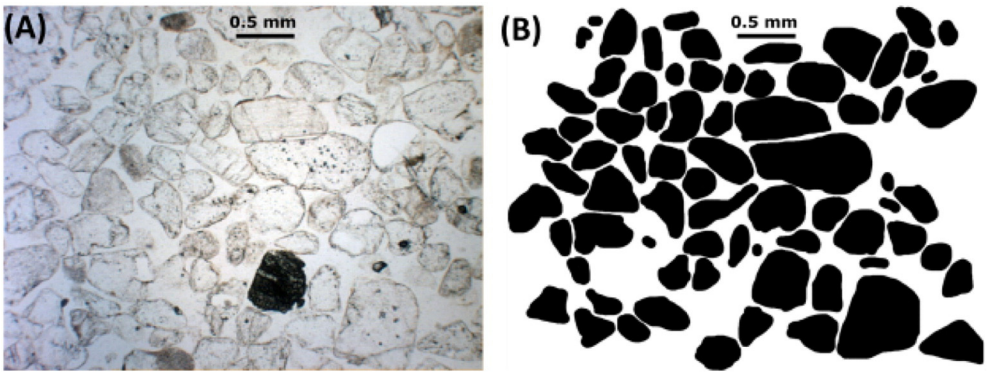

Fig. 9. An example of the sheared sediment collected at the end of experiment 1 after a shearing distance of 1280 cm. (A) Thin section of grains. (B) Black and white image analysis from thin section used to quantify grain orientation.

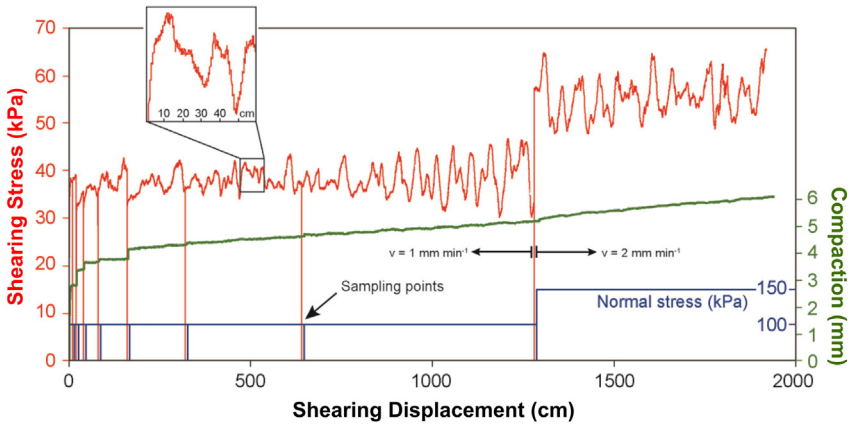

Fig. 10. Development of shear stresses and sediment compaction during the ring shear experiment 2 under normal stress of 100 kPa (0–1280 cm displacement) and 150 kPa (1280–1920 cm displacement). Note the shear stress heterogeneity evident during the entire experiment believed to have contributed to the variations in D_e distribution; v is the shearing velocity.

here demonstrates that measurement issues or sediment characteristics cannot account for the zero-dose grains measured. If pressure across bridges between grains is the key resetting mechanism for subglacial sediments and landforms then such conditions do not apply to other nonglacial environments. As such, findings from this work cannot be directly extended to non-glacial environments except for sediments in tectonic areas with active near-surface faults.

The observed increasing numbers of zero-dosed grains with shearing distance supports the original findings of Swift et al. (2011) that the lower measured luminescence signals of sediment sampled directly from the glacier bed beneath ~100 m of glacier at Haut Glacier d'Arolla, Switzerland, were attributable had been reset. As many glacial sediments will have been in the shearing zone for distance greatly exceeding that of this ring-shearing experiment, reset grains in many glacial diamicts and landforms may be more prevalent than previously thought. This may account for the relatively good resetting of sediment associated with glacial landforms that have been obtained as part of the BRITICE-CHRONO project (e.g., Evans et al., 2017; Smedley et al., 2017; Bateman et al., 2018). That many glacial studies have struggled in this regard may be more because of insensitive quartz and poor intrinsic OSL characteristics of local bedrocks (e.g., Sawakuchi et al., 2011; Klasen et al., 2016) than to lack of signal resetting. Future work requires targeting of natural subglacial sediments in regions that have quartz with good luminescence characteristics to establish whether robust chronologies from these depositional contexts are indeed possible. A resetting mechanism associated with active transport at the ice-bed interface may also offer potential as a glaciological process tracer. For example, the degree of resetting could be used to quantify sediment strain history or sediment residence times in contemporary systems (Swift et al., 2011).

5. Conclusions

- The occurrence of a small number of zero-dose grains in the shearing zone that increase in number with shearing confirms the preliminary findings of Bateman et al. (2012). Grains either appeared to retain their given dose or had a zero-dose.
- Data show that grain fracturing or loss of surface material is not responsible for OSL zeroing.
- Stress variations increased toward the end of the experiments with rapid changes in the order of 18 kPa within a few centimeters of shearing that are interpreted as the build up and collapse of grain bridges. The observed changes in grain characteristics are thought to have led to more bridging with increasing shear distance.
- Localised high pressure grain-to-grain stresses within bridges (or during their collapse) appear to explain why some grains become zeroed whilst other retain their palaeodose.
- Relatively short shearing distances might be sufficient to reset a small proportion of the luminescence signal within subglacial sediments. This opens up the potential for future work to successfully apply luminescence dating to sediments contained within subglacial landforms.

Acknowledgements

This work was funded through a Danish Agency for Science Technology and Innovation (FNU) grant 272-08-0492. Field sampling was

undertaken by DAS, MDB and JAP. Ring-shear experiments were carried out by JAP; sediment characterisation by DAS, JAP, and AD; with OSL measurements carried out by MDB. Rob Ashurst and Adam Dunajko are thanked for their assistance in sample preparation and sediment characterisation. Andrew Murray (Aarhus University) is thanked for enabling the gamma-irradiation to take place at Risø. David Sanderson (Scottish Universities Environmental Research Centre, East Kilbride, Scotland) is thanked for his generous input and guidance at the initial stages of this research. Peter Chung is thanked for providing access to the SEM facility at the Department of Geographical and Earth Sciences, University of Glasgow. Finally, we would like to thank the anonymous reviewer and the journal editor, whose detailed comments and thoughts have helped improve the final manuscript.

Appendix A. Supplementary data

Supplementary data to this article can be found online at https://doi.org/10.1016/j.geomorph.2018.01.017.

References

Aitken, M.J., 1985. Thermoluminescence Dating. Academic Press, London, p. 351.
Anjar, J., Larsen, N.K., Håkansson, L., Möller, P., Linge, H., Fabel, D., Xu, S., 2014. A ^{10}Be-based reconstruction of the last deglaciation in southern Sweden. Boreas 43, 132–148.
Ballantyne, C.K., 2010. Extent and deglacial chronology of the last British-Irish Ice Sheet: implications of exposure dating using cosmogenic isotopes. J. Quat. Sci. 25, 515–534.
Ballarini, M., Wallinga, J., Duller, G.A.T., Brouwer, J.C., Bos, A.J.J., Van Eijk, C.W.E., 2005. Optimizing detection filters for single-grain optical dating of quartz. Radiat. Meas. 40, 5–12.
Bateman, M.D., Boulter, C.H., Carr, A.S., Frederick, C.D., Peter, D., Wilder, M., 2007. Detecting post-depositional sediment disturbance in sandy deposits using optical luminescence. Quat. Geochronol. 2, 57–64.
Bateman, M.D., Carr, A.S., Dunajko, A.C., Holmes, P.J., Roberts, D.L., McLaren, S.J., Bryant, R.G., Marker, M.E., Murray-Wallace, C.V., 2011. The evolution of coastal barrier systems: a case study of the Middle-Late Pleistocene Wilderness barriers, South Africa. Quat. Sci. Rev. 30, 63–81.
Bateman, M.D., Catt, J.A., 1996. An absolute chronology for the raised beach deposits at Sewerby, E. Yorkshire, UK. J. Quat. Sci. 11, 389–395.
Bateman, M.D., Evans, D.J.A., Roberts, D.H., Medialdea, A., Ely, E., Clark, C.D., 2018. The timing and consequences of the blockage of the Humber Gap by the last British-Irish Ice Sheet. Boreas 47, 41–61.
Bateman, M.D., Frederick, C.D., Jaiswal, M.K., Singhvi, A.K., 2003. Investigations into the potential effects of pedoturbation on luminescence dating. Quat. Sci. Rev. 22, 1169–1176.
Bateman, M.D., Swift, D.A., Piotrowski, J.A., Sanderson, D.C.W., 2012. Investigating the effects of glacial shearing of sediment on luminescence. Quat. Geochronol. 10, 230–236.
Biegel, R.L., Sammis, C.G., Dieterich, J.M., 1989. The friction properties of a simulated gouge having a fractal distribution. J. Struct. Geol. 11, 827–846.
Bisschop, J., den Broka, B., Miletich, R., 2005. Brittle deformation of quartz in a diamond anvil cell. J. Struct. Geol. 27, 943–947.
Boulton, G.S., 1974. Processes and patterns of glacial erosion. In: Coates, D.R. (Ed.), Glacial Geomorphology (Proceedings of the Fifth Annual Geomorphology Symposia, Binghampton). Allen & Unwin, London, pp. 41–87.
Briant, R.M., Bateman, M.D., 2009. Luminescence dating indicates radiocarbon age underestimation in Late Pleistocene fluvial deposits from eastern England. J. Quat. Sci. 24, 916–927.
Clark, C.D., Hughes, A.L.C., Greenwood, S.L., Jordan, C., Sejrup, H.S., 2012. Pattern and timing of retreat of the last British-Irish Ice Sheet. Quat. Sci. Rev. 44, 112–146.
Clemmensen, L.B., Murray, A.J., Heinemeier, J., de Jong, R., 2009. The evolution of Holocene coastal dunefields, Jutland, Denmark: a record of climate change over the past 5000 years. Geomorphology 105, 303–313.
Cohen, D., Iverson, N.R., Hooyer, T.S., Fischer, U.H., Jackson, M., Moore, P.L., 2005. Debris-bed friction of hard-bedded glaciers. J. Geophys. Res. 110, F02007.
Crawford, E., Mortensen, J.K., 2009. An ImageJ plugin for the rapid morphological characterization of separated particles and an initial application to placer gold analysis. Comput. Geosci. 35, 347–359.
Cox, M.R., Budhu, M., 2007. A Practical Approach to Grain Shape Quantification. Eng. Geol. 96, 1–16.
Damsgaard, A., Egholm, D., Piotrowski, J.A., Tulaczyk, S., Larsen, N.K., Tylmann, K., 2013. Discrete element modeling of subglacial sediment deformation. J. Geophys. Res. Earth Surf. 118, 1–13.
Davis, P.T., Bierman, P.R., Corbett, L.B., Finkel, R., 2015. Cosmogenic exposure age evidence for rapid Laurentide deglaciation of the Katahdin area, west-central Maine, USA, 16 to 15 ka. Quat. Sci. Rev. 116, 95–105.
Dreimanis, A., Hutt, G., Raukas, A., Whippey, P.W., 1978. Dating methods of Pleistocene deposits and their problems: I. Thermoluminescence dating. Geosci. Can. 5, 55–60.
Drescher, A., de Josselin de Jong, G., 1972. Photoelastic verification of a mechanical model for the flow of a granular material. J. Mech. Phys. Solids 20, 337–351.
Duller, G.A.T., Bøtter-Jensen, L., Kohsiek, P., Murray, A.S., 1999. A high-sensitivity optically stimulated luminescence scanning system for measurement of single sand-sized grains. Radiat. Prot. Dosim. 84, 325–330.
Duller, G.A.T., Wintle, A.G., Hall, A.M., 1995. Luminescence dating and its application to key pre-late Devensian sites in Scotland. Quat. Sci. Rev. 14, 495–519.
Dyke, A.S., Andrews, J.T., Clark, P.U., England, J.H., Miller, G.H., Shaw, J., Veillette, J.J., 2001. The Laurentide and Innuitian ice sheets during the Last Glacial Maximum. Quat. Sci. Rev. 21, 9–31.
Evans, D.J.A., Bateman, M.D., Roberts, D.H., Medialdea, A., Hayes, L., Clark, C.D., 2017. Glacial Lake Pickering: stratigraphy and chronology of a proglacial lake dammed by the North Sea Lobe of the British-Irish Ice Sheet. J. Quat. Sci. 32, 295–310.
Fuchs, M., Owen, L.A., 2008. Luminescence dating of glacial and associated sediments: review, recommendations and future directions. Boreas 37, 636–659.
Fukuchi, T., 1989. Increase of radiation sensitivity of ESR centres by faulting and criteria of fault dates. Earth Planet. Sci. Lett. 94, 109–122.
Galbraith, R.F., Green, P.F., 1990. Estimating the component ages in a finite mixture. Radiat. Meas. 17, 197–206.
Gibbard, P.L., Pasanen, A.H., West, R.G., Lunkka, J.P., Boreham, S., Cohen, K.M., Rolfe, C., 2009. Late Middle Pleistocene glaciation in East Anglia, England. Boreas 38, 504–528.
Godfrey-Smith, D.I., Huntley, D.J., Chen, W.H., 1988. Optical dating studies of quartz and feldspar sediment extracts. Quat. Sci. Rev. 7, 373–380.
Gueydan, F., Mehl, C., Parra, T., 2005. In: Gapais, D., Brun, J.P., Cobbold, P.R. (Eds.), Stress-strain rate history of a midcrustal shear zone and the onset of brittle deformation inferred from quartz recrystallized grain size. 243. Geological Society, London, pp. 127–142 Special Publications.
Hamblin, R.J.O., Moorlock, B.S.P., Rose, J., Lee, J.R., Riding, J.B., Booth, S.J., Pawley, S.M., 2005. Revised pre-Devensian glacial stratigraphy in Norfolk, England, based on mapping and till provenance. Geol. Mijnb. 84, 77–85.
Hooke, R.L.B., Iverson, N.R., 1995. Grain-size distribution in deforming subglacial tills: role of grain fracture. Geology 23, 57–60.
Hooyer, T.S., Iverson, N.R., Lagroix, F., Thomason, J.F., 2008. Magnetic fabric of sheared till: a strain indicator for evaluating the bed-deformation model of glacier flow. J. Geophys. Res. 113, F02002.
Houmark-Nielsen, M., 2009. Testing OSL failures against a regional Weichselian glaciation chronology from southern Scandinavia. Boreas 37, 660–677.
Hughes, A.L.C., Gyllencreutz, R., Lohne, O.S., Mangerud, J., Svendsen, J.I., 2016. The last Eurasian ice sheets - a chronological database and time-slice reconstruction, DATED-1. Boreas 45, 1–45.
Iverson, N.R., Hooyer, T.S., Hooke, R.L., 1996. A laboratory study of sediment deformation: stress heterogeneity and grain size evolution. Ann. Glaciol. 22, 167–175.
Jenson, J.W., Clark, P.U., MacAyeal, D.R., Ho, C., Vela, J.C., 1995. Numerical modelling of advective transport of saturated deforming sediment beneath the Lake Michigan Lobe, Laurentide Ice Sheet. Geomorphology 14, 157–166.
King, G.E., Robinson, R.A.J., Finch, A.A., 2014. Towards successful OSL sampling strategies in glacial environments: deciphering the influence of depositional processes on bleaching of modern glacial sediments from Jostedalen, Southern Norway. Quat. Sci. Rev. 89, 94–107.
King, G.E., Sanderson, D.C.W., Robinson, R.A.J., Finch, A.A., 2014. Understanding processes of sediment bleaching in glacial settings using a portable OSL reader. Boreas 43, 955–972.
Klasen, N., Fiebig, M., Preusser, F., 2016. Applying luminescence methodology to key sites of Alpine glaciations in Southern Germany. Quat. Int. 28, 249–258.
Krumbein, W.C., 1941. Measurement and geological significance of shape and roundness of sedimentary particles. J. Sediment. Petrol. 11, 64–72.
Lamothe, M., 1988. Dating till using thermoluminescence. Quat. Sci. Rev. 7, 273–276.
Larsen, N.K., Piotrowski, J.A., Christiansen, F., 2006. Microstructures and microshears as proxy for strain in subglacial diamicts: implications for basal till formation. Geology 34, 889–892.
Larsen, N.K., Piotrowski, J.A., Menzies, J., 2007. Microstructural evidence of low-strain, time-transgressive subglacial deformation. J. Quat. Sci. 22, 593–608.
Lee, H.K., Schwarcz, H.P., 1994. Criteria for complete zeroing of ESR signals during faulting of the san Gabriel fault zone, southern California. Tectonophysics 235, 317–337.
Lee, J.R., Rose, J., Hamblin, R.J.O., Moorlock, B.S.P., Riding, J.B., Phillips, E., Barendregt, R.W., Candy, I., 2011. The glacial history of the British Isles during the Early and Middle Pleistocene: implications for the long-term development of the British ice sheet. Developments in Quaternary Science 15, 59–74.
Li, Y.R., Aydin, A., 2010. Behavior of rounded granular materials in direct shear: mechanisms and quantification of fluctuations. Eng. Geol. 115, 96–104.
Livingstone, S.J., Piotrowski, J.A., Bateman, M.D., Ely, J.C., Clark, C.D., 2015. Discriminating between subglacial and proglacial lake sediments: an example from the Dänischer Wohld Peninsula, northern Germany. Quat. Sci. Rev. 112, 86–108.
Livingstone, S.J., Roberts, D.H., Davies, B.J., Evans, D.J.A., O'Cofaigh, C., Gheorghiu, D.M., 2015. Late Devensian deglaciation of the Tyne Gap Palaeo-Ice Strean, northern England. J. Quat. Sci. 30, 790–804.
Mandl, G., de Jong, L.N.J., Maltha, A., 1977. Shear zones in granular material. Rock Mech. 9, 95–144.
Mark, D.M., 1973. Analysis of axial orientation data, including till fabrics. Geol. Soc. Am. Bull. 84, 1369–1374.
McCormack, D.C., Brocklehurst, S.H., Irving, D.H., Fabel, D., 2011. Cosmogenic 10Be insights into the extent and chronology of the last deglaciation in Wester Ross, northwest Scotland. J. Quat. Sci. 26, 97–108.
McKeever, S.W.W., 1985. Thermoluminescence of Solids. Cambridge University Press, Cambridge, p. 376.

Menzies, J., Gao, C., Kodors, C., 2013. Microstructural analyses of a Middle Pliocene till from the James Bay Lowlands, Canada—evidence of "potential" fast ice streaming. Proc. Geol. Assoc. 124, 790–801.
Morozov, G.V., 1968. The relative dating of Quaternary Ukrainian sediments by the TL method. VIIIth International Quaternary Association Congress, Paris. USGS Library, Washington, p. 167 Catalog No. 208 M8208.
Murray, A.S., Clemmensen, L.B., 2001. Luminescence dating of Holocene aeolian sand movement, Thy, Denmark. Quat. Sci. Rev. 20, 751–754.
Murray, A.S., Wintle, A.G., 2003. The single aliquot regenerative dose protocol: potential for improvements in reliability. Radiat. Meas. 37, 377–381.
Narloch, W., Piotrowski, J.A., Wysota, W., Larsen, N.K., Menzies, J., 2012. The signature of strain magnitude in tills associated with the Vistula Ice Stream of the Scandinavian Ice Sheet, central Poland. Quat. Sci. Rev. 57, 105–120.
Narloch, W., Piotrowski, J.A., Wysota, W., Tylmann, K., 2015. Till formation under a soft-bedded palaeo-ice stream of the Scandinavian Ice Sheet, constrained using qualitative and quantitative microstructural analyses. Sediment. Geol. 326, 64–78.
Paterson, W.S.B., 1994. The Physics of Glaciers. Butterworth & Heinemann, Oxford.
Pawley, S.M., Bailey, R.M., Rose, J., Moorlock, B.S.P., Hamblin, R.J.O., Booth, S.J., Lee, J.R., 2008. Age limits on Middle Pleistocene glacial sediments from OSL dating, north Norfolk, UK. Quat. Sci. Rev. 27, 1363–1377.
Powers, M.C., 1953. A new roundness scale for sedimentary particles. J. Sediment. Petrol. 23, 117–119.
Preusser, F., Blei, A., Graf, H.R., Schlüchter, C., 2007. Luminescence dating of Würmian (Weichselian) proglacial sediments from Switzerland: methodological aspects and stratigraphical conclusions. Boreas 36, 130–142.
Rhodes, E.J., 2000. Observations of thermal transfer OSL signals in glacigenic quartz. Radiat. Meas. 32, 595–602.
Rhodes, E.J., Bailey, R.M., 1997. Thermal transfer effects observed in the luminescence of quartz from recent glaciofluvial sediments. Quat. Sci. Rev. 16, 291–298.
Rhodes, E.J., Pownall, L., 1994. Zeroing of the OSL signal in quartz from young glaciofluvial sediments. Radiat. Meas. 23, 581–585.
Rittenour, T.M., Riggs, N.R., Kennedy, L.E., 2012. Application of single-grain OSL to date quartz xenocrysts within a basalt flow, San Francisco volcanic field, northern Arizona, USA. Quat. Geochronol. 10, 300–307.
Rodnight, 2008. How many equivalent dose values are needed to obtain a reproducible distribution? Ancient TL 26, 3–9.
Roussillon, T., Piégay, H., Sivignon, I., Tougne, L., Lavigne, F., 2009. Automatic computation of pebble roundness using digital imagery and discrete geometry. Comput. Geosci. 35, 1992–2000.
Sawakuchi, A.O., Blair, M.W., DeWitt, R., Faleiros, F.M., Hyppolito, T., Guedes, C.C.F., 2011. Thermal history versus sedimentary history: OSL sensitivity of quartz grains extracted from rocks and sediments. Quat. Geochronol. 6, 261–272.
Smedley, R.K., Scourse, J.D., Small, D., Hiemstra, J.F., Duller, G.A.T., Bateman, M.D., Burke, M.J., Chiverrell, R.C., Clark, C.D., Davies, S.M., Fabel, D., Gheorghiu, D.M., McCarroll, D., Medialdea, A., Xu, S., 2017. New age constraints for the limit of the British-Irish Ice Sheet on the Isles of Scilly. J. Quat. Sci. 32, 48–62.
Sohbati, R., Murray, A.S., Jain, M., Buylaert, J.-P., Thomsen, K.J., 2011. Investigating the resetting of osl signals in rock surfaces. Geochronometria 38, 249–258.
Spencer, J.Q.G., Hadizadeh, J., Gratier, J.-P., Doan, M.-L., 2012. Dating deep? Luminescence studies of fault gouge from the San Andreas Fault zone 2.6 km beneath Earth's surface. Quat. Geochronol. 10, 280–284.
Swift, D.A., Sanderson, D.C.W., Nienow, P.W., Bingham, R.B., Cochrane, I.C., 2011. Anomalous luminescence of subglacial sediment at Haut Glacier d'Arolla, Switzerland – a consequence of resetting at the glacier bed. Boreas 40, 446–458.
Takeuchi, A., Nagahama, H., Hashimoto, T., 2006. Surface resetting of thermoluminescence in milled quartz grains. Radiat. Meas. 41, 826–830.
Thrasher, I.M., Mauz, B., Chiverrell, R.C., Lang, A., Thomas, G.S.P., 2009. Testing an approach to OSL dating of late Devensian glaciofluvial sediments of the British Isles. J. Quat. Sci. 24, 785–801.
Toucanne, S., Soulet, G., Freslon, N., Silva Jacinto, R., Dennielou, B., Zaragosi, S., Eynaud, F., Bourillet, J.-F., Bayon, G., 2015. Millennial-scale fluctuations of the European Ice Sheet at the end of the last glacial, and their potential impact on global climate. Quat. Sci. Rev. 123, 113–133.
Toyoda, S., Rink, W.J., Schwarcz, H.P., Rees-Jones, J., 2000. Crushing effects on TL and OSL on quartz: relevance to fault dating. Radiat. Meas. 32, 667–672.
White, T.S., Bridgland, D.R., Westaway, R., Howard, A.J., White, M.J., 2010. Evidence from the Trent terrace archive, Lincolnshire, UK, for lowland glaciation of Britain during the Middle and Late Pleistocene. Proc. Geol. Assoc. 121, 141–153.
White, T.S., Bridgland, D.R., Westaway, R., Straw, A., 2016. Evidence for late Middle Pleistocene glaciation of the British margin of the southern North Sea. J. Quat. Sci. 32, 261–275.
Wright, J.S., 1995. Glacial comminution of quartz sand grains and the production of loessic silt: a simulation study. Quat. Sci. Rev. 14, 669–680.
Zöller, L., Blanchard, H., McCammon, C., 2009. Can temperature assisted hydrostatic pressure reset the ambient TL of rocks? – a note on the TL of partially heated country rock from volcanic eruptions. Ancient TL 27, 15–22.